



Uniform corrosion of FeCrAl cladding tubing for accident tolerant fuels in light water reactors

Liang Yin, T.B. Jurewicz, M. Larsen, M. Drobniak, C.C. Graff, D.R. Lutz¹, R.B. Rebak*

GE Research, Schenectady - NY, 12309 USA



ARTICLE INFO

Article history:

Received 31 December 2020

Revised 10 May 2021

Accepted 13 May 2021

Available online 24 May 2021

Keywords:

Accident tolerant fuel

FeCrAl cladding

Corrosion resistance

Steam oxidation resistance

Oxide film

ABSTRACT

Iron-Chromium-Aluminum (FeCrAl) alloys are candidate materials for light water reactor accident tolerant fuel (ATF) rod cladding because of the unparalleled resistance of these alloys to attack by superheated steam in the case of a loss of coolant accident. Since FeCrAl alloys were never used before in a reactor environment, it was important to characterize their corrosion resistance under simulated reactor normal operation conditions. Tests were conducted for APMT and C26M alloys in three ~300°C water systems (two containing hydrogen and one containing oxygen). Results show that after 12 months of immersion the FeCrAl alloys lose a small amount of mass. The resistance to corrosion is mostly given by the development on the surface of a protective oxide mostly rich in Cr and Al. The mass loss was lower in APMT than in C26M because of the higher Cr content in the former. After 12 months residence in the ~300°C water, the FeCrAl specimens maintained their unequalled resistance to attack by 1200°C steam.

© 2021 The Author(s). Published by Elsevier B.V.
This is an open access article under the CC BY-NC-ND license
(<http://creativecommons.org/licenses/by-nc-nd/4.0/>)

1. Introduction

The hydrogen explosions at the Fukushima Daiichi site of the nuclear power stations accelerated the development of accident tolerant fuels (ATF) [10,12]. ATF materials include components for the fuel itself and for the cladding. There are three main global concepts being proposed for the cladding, which in order of readiness for reactor service are; (1) coated zirconium alloys, (2) monolithic FeCrAl alloys, and (3) Silicon Carbide composite materials [10]. In the USA the three fuel vendors are working in the development of coated zirconium alloys and silicon carbide composites. Only one fuel vendor is also developing the monolithic FeCrAl alloys. The FeCrAl or Kanthal alloys are a 90-years old family of ferritic alloys containing approximately 20% Cr and 5% Al, which gives them extraordinary resistance to attack by high temperature air and steam. Since the failure of the fuel clad with zirconium alloys at the Fukushima Daiichi stations was due to attack by superheated steam, the idea of using FeCrAl alloys for the cladding seems logical [4,5,10,12,15,16]. A cladding material candidate not only has to behave well under steam or loss of coolant accident conditions but also be viable in the entire fuel cycle, including cost

effective tube fabrication, residence in reactor condensed water for up to ten years, residence in used fuel cooling pools and finally dry cask storage plus reprocessing or used fuel geologic disposal [9].

Previous research has shown that FeCrAl alloys including APMT, C26M and other variants were resistant to corrosion in high temperature water with several chemistries and temperatures in the order of 300°C [2,3,7,11,13,14]. The resistance to corrosion of ferritic FeCrAl alloys in high temperature water is not surprising since FeCrAl contain enough Cr to provide passivation in the same manner as the 70 year old nuclear materials type 304/316 austenitic stainless steel remain passive. Studies of the passive film developed on the surface of the FeCrAl alloys exposed to ~300°C water showed that a Cr rich film is always present for protection [3,6,11]. This Cr rich film may be only a few nanometers thick and is present adjacent to the uncorroded metal and underneath a thicker film which would be mostly rich in iron [3,6].

The objective of the current research was to determine the corrosion behavior for up to one year immersion of typical BWR geometry FeCrAl cladding tubing in three simulated water chemistries at 288°C and at 330°C. The one-year tube specimens were subsequently tested in steam at 1200°C.

2. Experimental method

Two chemical compositions of FeCrAl alloys were immersion corrosion tested along with the current commercial nuclear power

* Corresponding author.

E-mail addresses: rebak@ge.com, rrebak@aol.com (R.B. Rebak).

¹ GE Power, Sunol - CA, 94586 USA

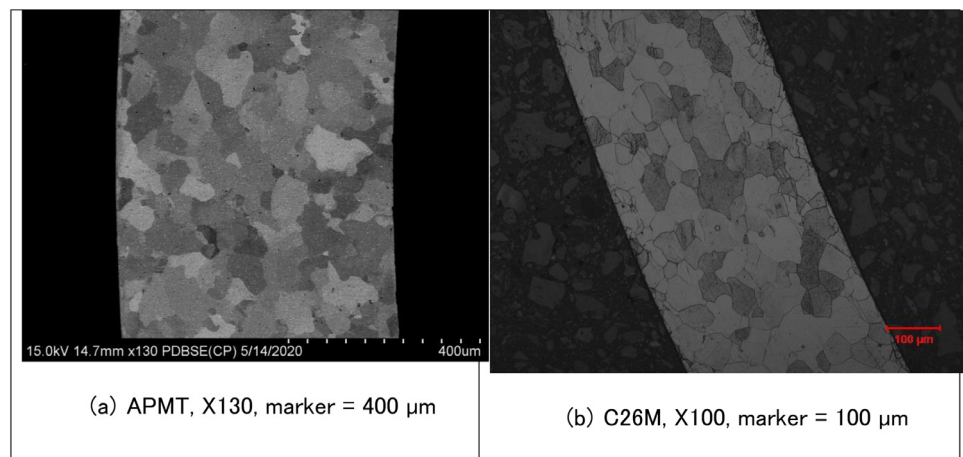


Fig. 1. Typical microstructure of the tested tubes of APMT and C26M. The wall thickness of APMT tube was ~600 μm , and the wall thickness of the C26M tube was ~400 μm . Both APMT and C26M tubes had a fully recrystallized microstructure.

Table 1
Nominal chemical composition of IronClad FeCrAl alloys
in mass percent.

Alloy	Cr	Al	Others
Zirc-2	0.1	-	Bal Zr, 1.4Sn, 0.05Ni, 0.12Fe
APMT	21	5	Bal Fe, 3Mo, Y, Zr, Ti
C26M	12	6	Bal Fe, 2Mo, 0.05Y

plant cladding material of Zircaloy-2. **Table 1** gives the nominal compositions of the three studied alloys. The C26M tubes were made using an earlier process of traditional metallurgy (melting, casting and forging) before tube making. The wall thickness for C26M was targeted to be 0.4 mm. Actual C26M specimens wall thickness measurements in 36 locations showed an average wall thickness of $405.93 \pm 5.15 \mu\text{m}$. Similarly, the APMT specimens were an earlier version which followed the traditional fabrication practice, with an intended nominal wall thickness of 0.6 mm. Actual APMT specimen wall thickness measurements in 36 locations showed an average value of $584.38 \pm 13.29 \mu\text{m}$. The average wall thickness for the Zirc-2 specimens, including the ID liner, was $675.71 \pm 6.38 \mu\text{m}$. The immersion corrosion tube specimens were nominally 10 mm long sections of actual cladding geometry with 10.26 mm OD. The approximate mass of the Zirc-2, APMT, and C26M tube specimens were approximately 1.24 g, 1.21 g and 0.87 g, respectively, and the total exposed surface area of each specimen (including OD and ID surfaces) was in the order of 6 cm^2 . The APMT tube was made following the typical pre-optimization powder metallurgy technology which yielded recrystallized grains, dispersed oxides (shown as submicron white dots), and some sporadic porosity (**Fig. 1a**). The C26M tubing was also an earlier version of this alloy following the traditional melting, casting, and forging process which yielded slightly larger grains but without porosity or abundantly dispersed particles (**Fig. 1b**). Currently both APMT and C26M tubing are being processed following powder metallurgy technology and pilgering tube making procedures. The newer tube meets nuclear cladding requirements with an optimized wall thickness for neutral neutron penalty (as compared to Zirc-2 thicker cladding wall).

Three specimens of each alloy were tested in each autoclave system. Initially each autoclave contained 9 tube specimens (three for each alloy). One specimen from each alloy in each autoclave was removed at 6 months immersion for oxide surface characterization. Two specimens of each alloy in each autoclave were carried to 12-months exposure. The operating conditions of the autoclave systems are given in **Table 2**. The specimens were cleaned, de-

Table 2
Three testing conditions.

Autoclave	Test Conditions, One Year Immersion
S2	Simulated PWR, High Purity Water, 3.75 ppm H ₂ , 330°C
S5	Simulated BWR, Hydrogen Chemistry HWC (0.3 ppm H ₂), 288°C
S6	Simulated BWR, Normal Chemistry NWC (1 ppm O ₂), 288°C

greased, and weighed three times (m_i) before the immersion tests started. After each period of 3 months, the specimens were again cleaned and weighed three times (m_f). The mass change (gain or loss) was calculated as $m_f - m_i$ and then divided by the total initial exposed surface area of the specimens. The values of corrosion are reported as mg/cm². To convert this unit into mg/dm², multiply the value in mg/cm² by 100.

The testing conditions in **Table 2** were selected to represent a range of environmental conditions with oxygen or hydrogen at the same temperature (S5 & S6) or hydrogen condition with higher temperature (S2). The conditions are for near pure water, without adjusting pH values using lithium hydroxide or boric acid. The S2 autoclave (simulated PWR temperature) and S5 autoclave (simulated BWR temperature) had excess of dissolved hydrogen in the water which generated a corrosion potential for Zirc-2, APMT and C26M specimens of approximately -650 to -700 mV in the standard hydrogen electrode (SHE) scale. The S6 autoclave had an excess of 1 ppm dissolved oxygen and simulated BWR normal water chemistry that is oxidizing in nature, generating a corrosion potential of approximately -200 mV for Zirc-2 and 0 mV for APMT and C26M [8]. That is, the oxidation power of the environment in autoclave S6 was 500 to 700 mV higher than in autoclaves S2 and S5.

The immersion testing was performed using three separate autoclaves (**Table 2**), each one with their own water board circulating at a rate of 200 cm³/min, which represents two replenishments of each autoclave every hour. The high purity water was preconditioned with the right gas amount in a 4-L glass column from which the water was drawn and pumped through the autoclave using a high pressure pump. The pressure was controlled by a back pressure regulator at approximately 10 MPa (higher for the PWR simulated system). The water was continuously filtered at the exit of the autoclave. The conductivity of the water was continuously monitored before entering the autoclave and as it exited the autoclave. In the PWR S2 system the typical ingress water resistivity (conductivity) was 17.5 MΩ, and the egress was 10.8 MΩ. In the BWR HWC S5 system the ingress water was 18 MΩ and the egress was 12.4 MΩ. In the BWR NWC S6 system the ingress water was

18 MΩ and the egress was 8.1 MΩ. The lower resistance in the S6 system egress water shows that this oxygen containing system was the most aggressive since it produced more dissolved species. Data also shows that the filtering system in the outlet of the autoclaves worked well.

Steam tests were performed at ambient pressure in a system having 100% steam at 1200°C for 2 h or 4 h of testing. The coupons were cleaned, dimensioned, and weighed three times before exposure to steam and weighed again after steam exposure. The mass change was calculated in the same manner as for the autoclave immersed specimens.

After the water immersion tests and the steam tests the specimens were carefully characterized by using optical imaging, secondary electron scanning electron microscopy (SEM) surface imaging, X-ray photoelectron spectroscopy (XPS) analysis and transmission electron microscopy (TEM) of across the surface oxide lifted samples obtained by Focus Ion Beam (FIB) cutting. X-ray photoelectron spectroscopy (XPS) was used to characterize the chemical composition of the surface oxide films after the immersion testing. By irradiating the surface with an X-ray beam, the photoelectron emission from the top 1–10 nm of surface was measured. The XPS analyses were performed on a KRATOS Axis Ultra DLD XPS system using an Al K α radiation (1486.6 eV) at 225 W. The analysis area employed for the as-received surfaces was ~700 × 300 μm . After the as-received surface was analyzed, Ag+ ion sputtering of the surface for 60 s was conducted to remove the outermost surface layers ~1–2 nm, then XPS analysis was performed again. Once the elements were identified by the two surface surveys, high resolution core level spectra were collected using a pass energy of 20 eV. All the spectra were energy adjusted based on the C1s line for the hydrocarbon at 284.6 eV.

TEM analysis was conducted to characterize the morphology and composition of the surface oxides on the Zirc-2, APMT, and C26M tube specimens after 12 months immersion. The TEM specimens were prepared via a focus ion beam (FIB) cut and subsequent lift. The analysis was performed using Titan Themis S/TEM in transmission. Energy Dispersive Spectroscopy (EDS) elemental mapping was conducted to evaluate the element distribution inside the surface oxide films. For brevity sake, here we report results only for the specimens tested in the BWR NWC (S6) condition.

2.1. Experimental results and discussion

Figs. 2–4 show the mass change as a function of immersion time for the specimens immersed in the environments of autoclaves S2, S5, and S6, respectively. In the three autoclave systems the Zirc-2 tube specimens always slightly gained mass and the FeCrAl tube specimens slightly lost mass. In the three environments the mass loss was higher for the C26M specimens than for the APMT specimens probably because of the lower content of chromium in the C26M alloy composition (Table 1). Comparing data from Figs. 2 & 3 (both hydrogenated environments), the mass loss for the FeCrAl specimens was lower at 330°C (autoclave S2) than at 288°C (autoclave S5). In a hydrogenated environment it would be more difficult to form a protective chromium oxide on the surface than in an oxygenated environment. Fig. 4 shows that the mass loss for FeCrAl in the oxygenated environment was lower than in the hydrogenated water (Figs. 2 & 3).

Fig. 5 shows the mass change (gain) as a function of immersion time for the Zirc-2 tube specimens in the three autoclave systems. Fig. 5 shows that the largest mass gain for the Zirc-2 specimens was in the oxygenated water of autoclave S6, and the lowest was in BWR HWC conditions of autoclave S5. It is commonly accepted that a mass gain of 0.15 mg/cm² in a zirconium alloys represents a zirconium oxide (ZrO₂) thickness of 1 μm [1].

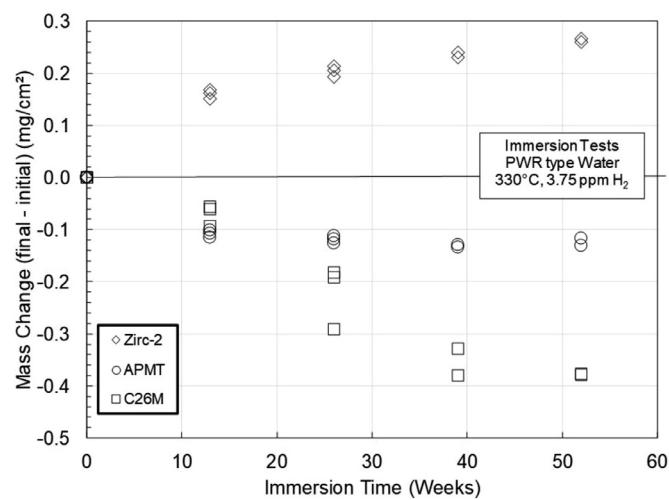


Fig. 2. Mass change as a function of immersion time for Zirc-2, APMT, and C26M tube specimens in simulated PWR hydrogenated water at 330°C (S2 in Table 2).

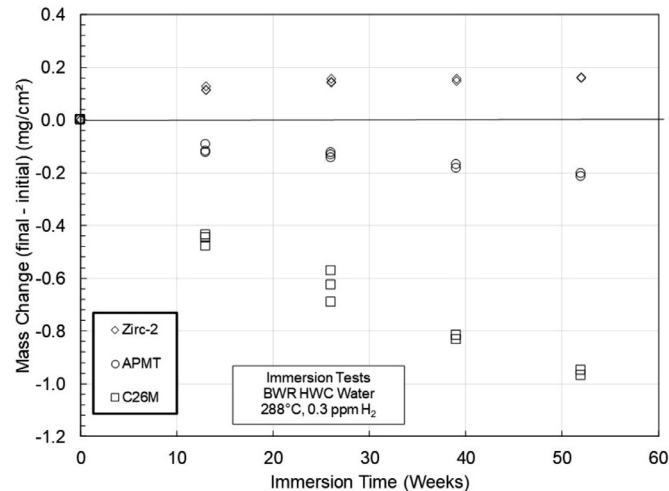


Fig. 3. Mass change as a function of immersion time for Zirc-2, APMT, and C26M tube specimens in simulated BWR hydrogenated water at 288°C (S5 in Table 2).

Fig. 6 shows the mass change (loss) as a function of immersion time for the APMT tube specimens in the three autoclave systems. The corrosion resistance of APMT in the high temperature water is given by the ability of the alloy to form a protective chromium oxide film on the surface. The more protective (continuous and defect free) this chromium oxide, the lower the mass loss. Fig. 6 shows that the lowest mass loss for APMT was for the S6 autoclave which contained a 1 ppm dissolved oxygen in the system, which promoted the oxide formation and therefore it limited the mass loss. The highest mass loss was in the S5 autoclave, which contained hydrogen at 288°C. After a year of testing the maximum mass loss for APMT in the three autoclaves was approximately 0.2 mg/cm². Considering the density of APMT to be 8 g/cm³, a mass loss of 0.2 mg/cm² represents a thinning of the tube of 0.25 μm [7].

Fig. 7 shows the mass change (loss) as a function of immersion time for C26M tube specimens in the three simulated high temperature reactor water conditions. The behavior of C26M specimens was like that of APMT specimens, following the same ranking. That is, the lowest mass loss for C26M was in the oxygenated water (system S6) and the highest mass loss was in the BWR HWC system. However, while the maximum mass loss for APMT (Fig. 6) was 0.2 mg/cm² in autoclave S5, the maximum mass loss after one year immersion for C26M was in the order of 1 mg/cm² or five

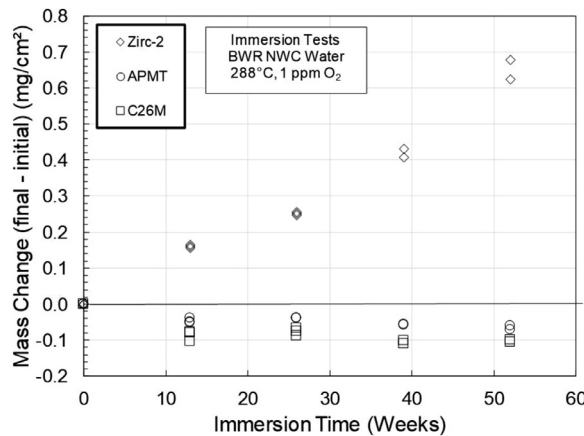


Fig. 4. Mass change as a function of immersion time for Zirc-2, APMT, and C26M tube specimens in simulated BWR oxygenated water at 288°C (S6 in Table 2).

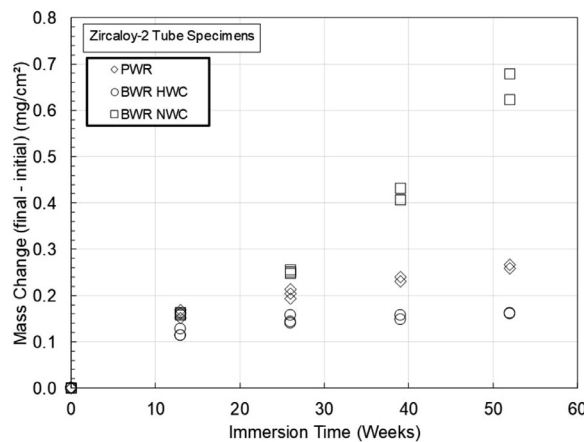


Fig. 5. Mass change as a function of immersion time for Zircaloy-2 tube specimens in simulated PWR, BWR HWC, and BWR NWC waters.

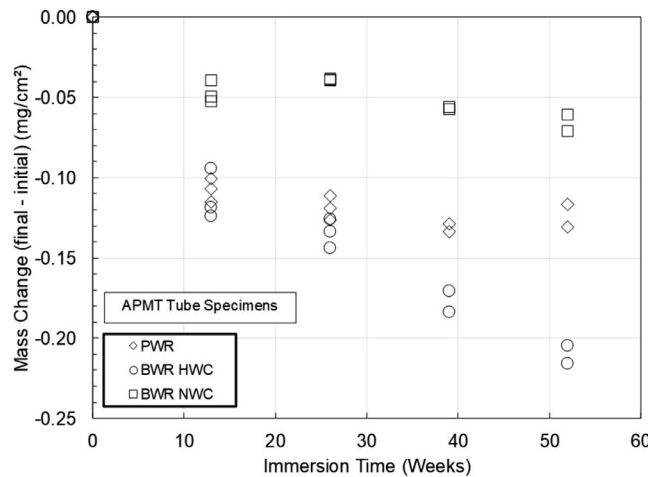


Fig. 6. Mass change as a function of immersion time for APMT tube specimens in simulated PWR, BWR HWC, and BWR NWC waters.

times higher than for APMT. This would represent a thinning of the C26M tube wall of 1.25 μm.

Water chemistry affects the duplex oxide structure and growth kinetics:

- a Among the three water chemistries, the BWR-NWC showed the least weight loss for both FeCrAl alloys, suggesting (aided by oxygen) the earliest formation of a protective Cr-rich inner lay-

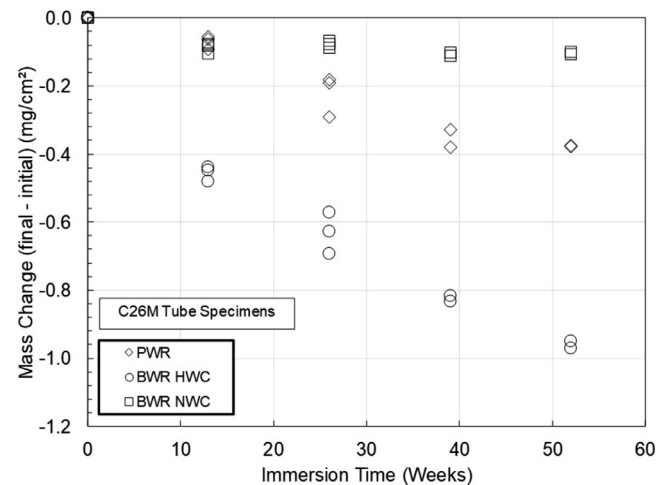


Fig. 7. Mass change as a function of immersion time for C26M tube specimens in simulated PWR, BWR HWC, and BWR NWC waters.

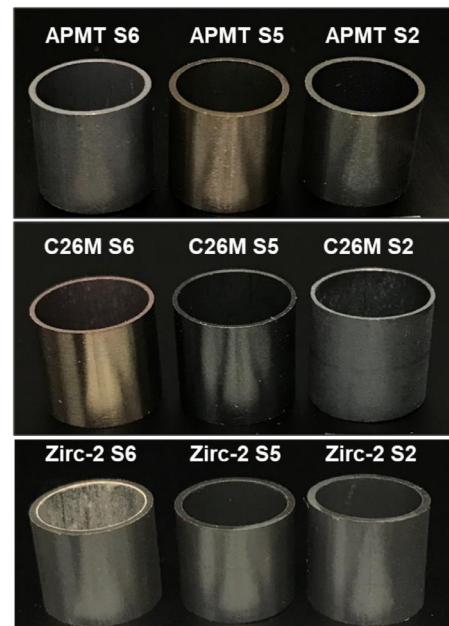


Fig. 8. Optical characteristics of the tube coupons for Zirc-2, APMT, and C26M after 12-month immersion in the three autoclave systems (Table 2).

ers in the oxygenated water. This barrier of Cr limited further dissolution of the cladding into the water.

b BWR-HWC showed the largest weight loss probably related to the slowest formation of a protective inner oxide layer due to the reducing environment and not sufficiently high temperature.

c PWR exhibited lower weight loss than BWR-HWC because of the increased water temperature of 330°C, which offered faster kinetics and faster oxide growth on the metal surface compared to BWR HWC.

2.2. Characteristics and composition of surface oxides

Optical - Fig. 8 shows the optical image characteristics of the 12-month tested tube specimens in the three autoclave systems S2, S5, and S6. Zirc-2 tube specimens have the characteristic black/blue lustrous oxide on the OD suggesting the formation of a protective ZrO₂ on the surface. The specimen exposed to the S6 system (oxidizing), had also considerable oxidation in the ID of the

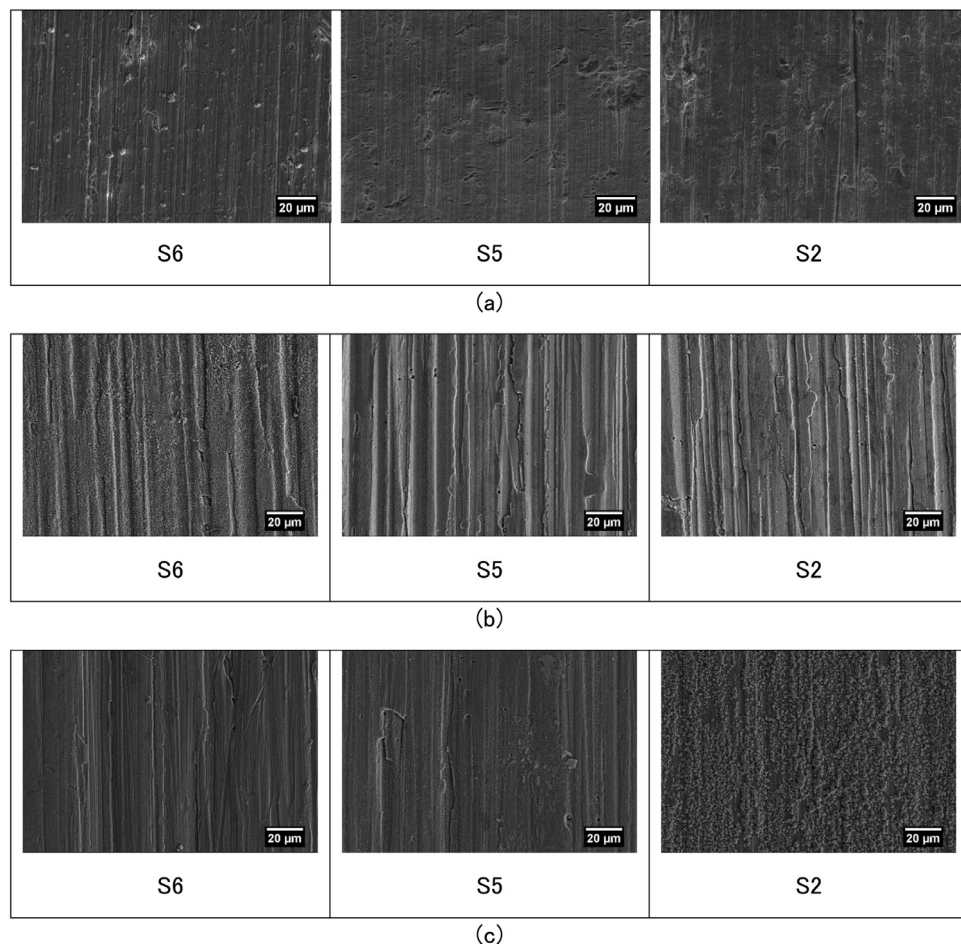


Fig. 9. Scanning Electron Microscopy X2000 appearance of the tube coupons for (a) Zirc-2, (b) APMT, and (c) C26M after 12-month immersion in the three autoclave systems (Table 2).

specimen, shown as a white oxide. This internal oxidation observation is a confirmation of the Fig. 5 higher mass gain for the BWR NWC system than for the two systems containing reducing hydrogen (PWR and BWR HWC). In its actual fuel rod application performance, the ID of the cladding would never be exposed to the coolant chemistry.

The APMT tube specimens had distinctive coloring (Fig. 8) depending on the environment exposed (Table 2). In the BWR NWC system (S6) the optical image shows a shiny gray silvery appearance. In the BWR HWC (S5) system the surface appearance was golden and in the PWR (S2) there was a color mixture between lustrous gray and shiny golden.

The C26M tube specimens also had distinctive coloring in the three tested water chemistries (Fig. 8). But the appearance of C26M specimens was different from the APMT specimens. For C26M, the tube exposed to the BWR NWC system was golden and in the PWR (S2) system the specimen was dull gray. The C26M tube had a shiny gray/black appearance in the S5 or BWR HWC system. The noticeable difference in the appearance of the two FeCrAl tubes is tied to their chemical composition (Table 1), especially to the Cr content, which is higher in APMT than in C26M.

Scanning Electron Microscopy SEM – Fig. 9 shows the appearance of the OD of the tested tube specimens in the three autoclave systems. Fig. 9a is for Zirc-2, Fig. 9b is for APMT and Fig. 9c is for C26M. The images for the surfaces of the Zirc-2 specimens (Fig. 9a) show little or no difference between them, as suggested by Fig. 8.

For the two FeCrAl tube specimens, the surfaces that showed a dull gray appearance in the optical images (APMT in S6 and C26M in S2) had noticeable amount of crystals or a non-smooth corrosion pattern on the surface (Figs. 9b, 9c and Fig. 10). The crystals observed on the surface are formed by reprecipitation of dissolved metal ions from the autoclave water environment.

The golden optical surface appearance of APMT in S5 and C26M in S6 seem to share a softer velvety and without surface crystals surface under 8000X SEM imaging (Fig. 11).

2.2.1. XPS analyses -

Results for APMT coupons exposed for 12-month under PWR, HWC and BWR conditions show that after sputtering, the C content was reduced significantly for all the coupons, while Al also decreased. Signals for O and Fe were common for all three coupons, while Cr, Al, Ni and Mo were detected for both PWR and HWC coupons (both hydrogenated water environments). The BWR NWC coupon did not show detectable Cr, Al or Ni. FeCrAl do not have Ni, therefore the nickel content observed on top of some of the tested coupons is originated from the slow corrosion of the equipment itself (autoclave, valve and piping) that is not fully filtered.

Results for C26M coupons tested alongside APMT coupons, showed that after sputtering, the C and Al content decreased. All three coupons had O, Fe and Ni. The BWR coupon did not show detectable Al and Ni. The largest difference between the base composition of APMT and C26M alloys is in the content of Cr, 21% ver-

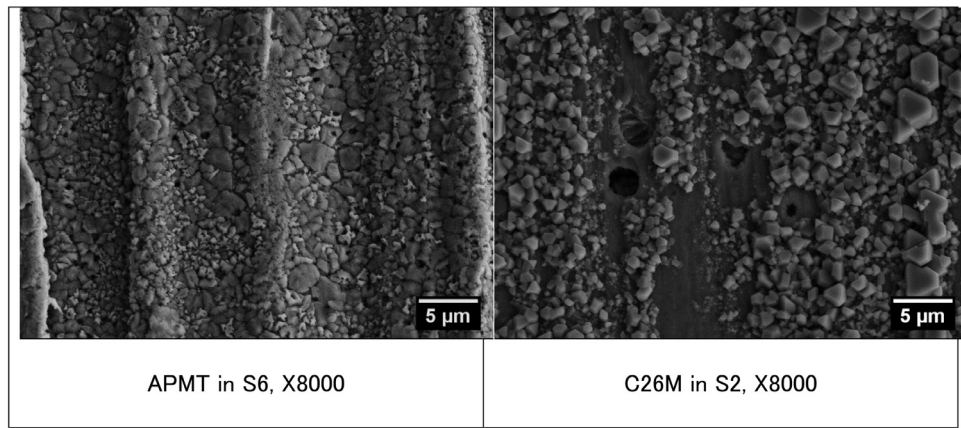


Fig. 10. SEM 8000X magnification of the surface of APMT and C26M specimens showing non-smooth surfaces giving the specimens a dull gray appearance.

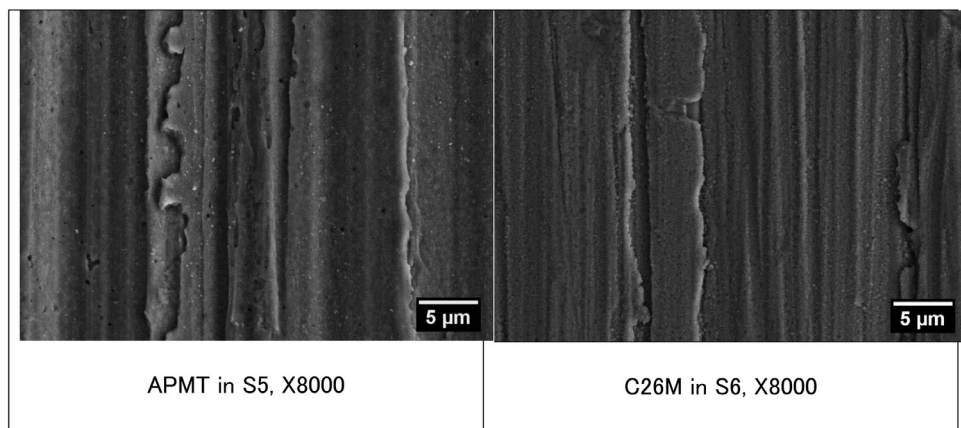


Fig. 11. SEM 8000X magnification of the surface of APMT and C26M specimens showing soft surfaces giving the specimens a golden appearance.

sus 12%, respectively. For PWR and HWC conditions, the surface Cr contents were higher in the APMT coupons after sputtering, 11.6% and 15.2% respectively, while C26M coupons had 2.2% and 10%. The trend overall was consistent with the initial Cr in the alloys. However, for the BWR NWC condition APMT did not show Cr on the surface but C26M had 1.4%.

Both APMT and C26M have ~5-6% Al in their base composition. For PWR and HWC conditions, the surface Al contents were similar between the two alloys, at about 3% after sputtering. Interestingly, for the BWR NWC condition both alloys did not show noticeable Al on the as-tested surface and after sputtering. XPS results suggest that the surface crystals observed in Fig. 10 are iron based. According to XPS, it is also likely that the smooth surface oxides without precipitated crystals corresponds to the presence of chromium oxide. The golden appearance could be a result of higher valence oxidized chromium.

2.2.2. TEM analyses-

Fig. 12 shows TEM analysis of the APMT specimen after immersion in BWR NWC (S6) for 12 months. The TEM bright field image shows the morphology and total thickness of the surface oxides between 194 nm to 390 nm. The EDS measurements show that the oxide was composed of two layers, an internal layer which is approximately 10-30 nm thick and an external layer approximately ten times thicker than the internal layer. The internal layer was mostly enriched in Cr but may also contained Al mainly in the

area between the metal and the Cr_2O_3 . The presence of Al along Cr in the internal layer was also reported by Raiman et al [3]. The external layer was mostly iron with some localized regions rich in Cr (Fig. 12). There is no Mo in the oxide. The 12-month test show that even at ~300°C aluminum oxide may selectively develop between the chromium oxide and the metal substrate probably following a similar mechanism as for high temperature (~1000°C) steam attack [5]. The immersion corrosion testing of APMT in ~300°C water shows that Cr will protect the FeCrAl alloy against corrosion, in the same manner as it protects the well known type 304/316SS. The other elements in the FeCrAl (Al and Mo) do not play a significant role in the performance of the FeCrAl alloy in water.

Fig. 13 shows the thickness and composition of the oxides formed on the C26M tube specimen. The oxide on C26M was about half the thickness of the oxide formed on APMT under the same tested conditions (Fig. 12). The oxide on C26M was also a double layer with a total thickness of approximately 150 nm, of which about 50 nm was the inner layer rich in Cr and Al (Fig. 13).

Fig. 14 shows the thickness and composition of the oxide formed on the OD of the tube of Zirc-2 after 12-month immersion in autoclave S6 or BWR NWC. The oxide thickness is approximately 1 μm thick. The surface oxide is entirely ZrO_2 , and may contain unoxidized particles rich in Cr, Fe and Ni called second phase particles (SPP) [7]. The distribution of the SPP is randomly the same in the substrate as in the oxide.

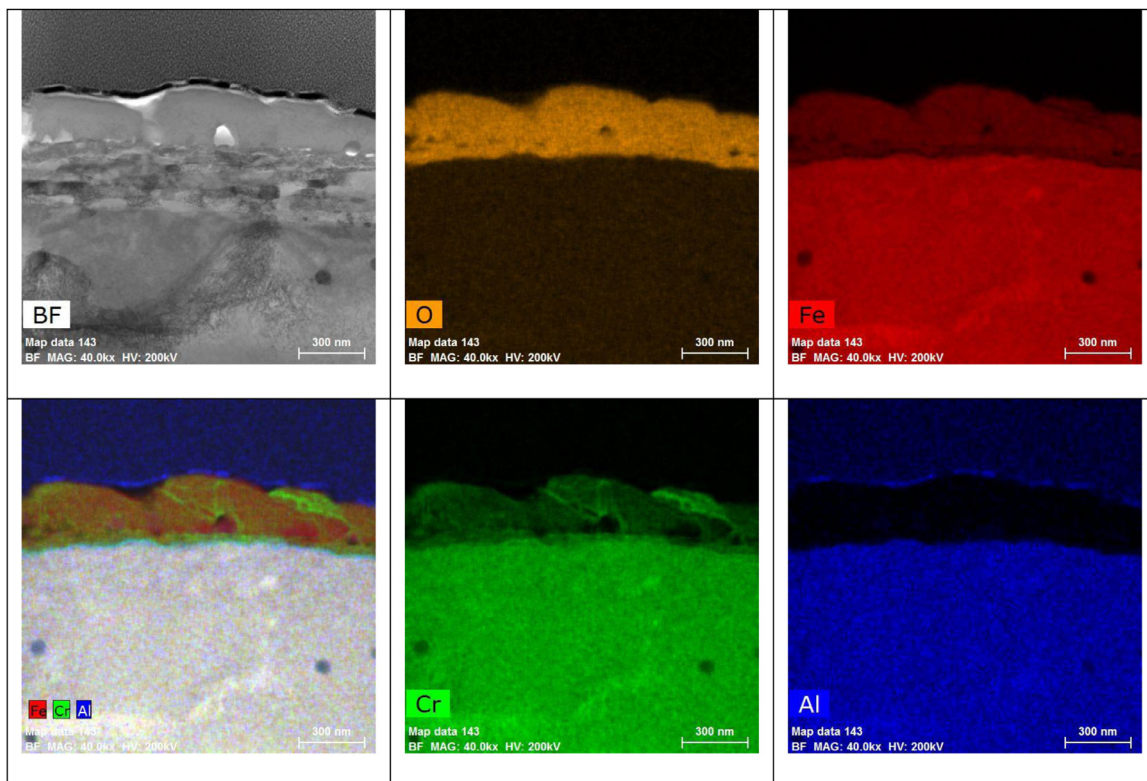


Fig. 12. TEM oxide cross section for APMT surface oxides formed after 12 months exposure in autoclave S6 or BWR NWC. The marker is 300 nm long.

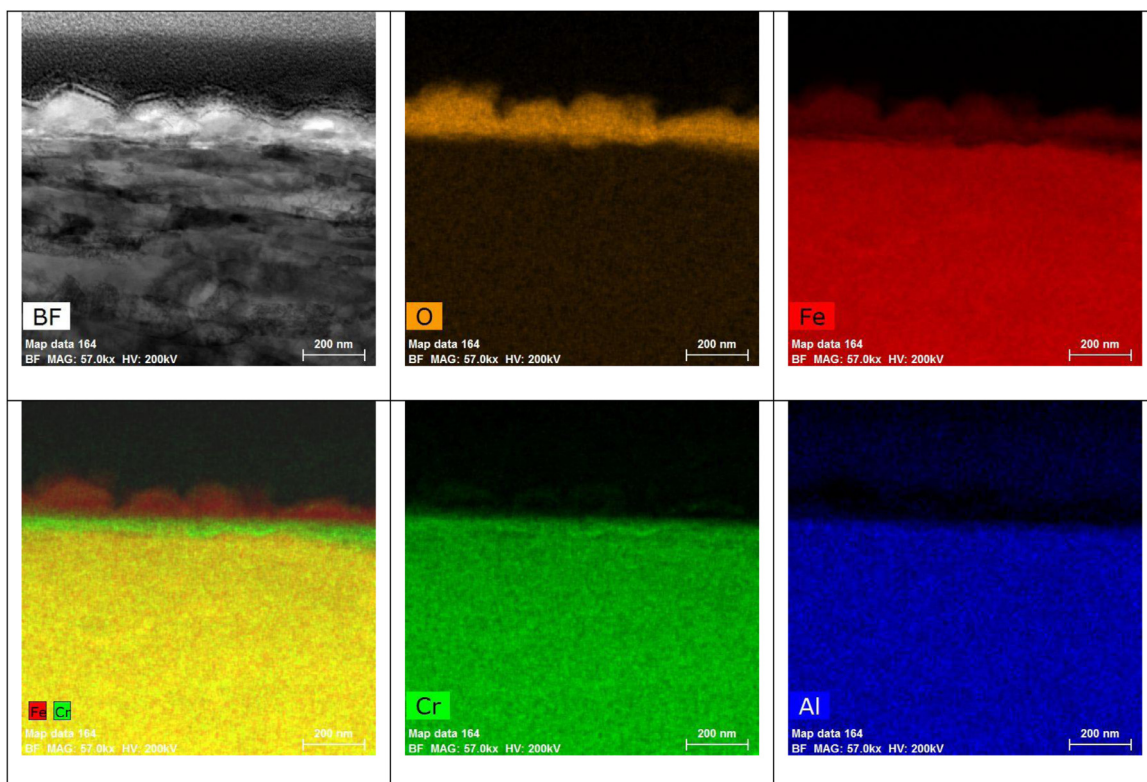


Fig. 13. TEM oxide cross section for C26M surface oxides formed after 12 months exposure in autoclave S6 or BWR NWC. The marker is 200 nm long.

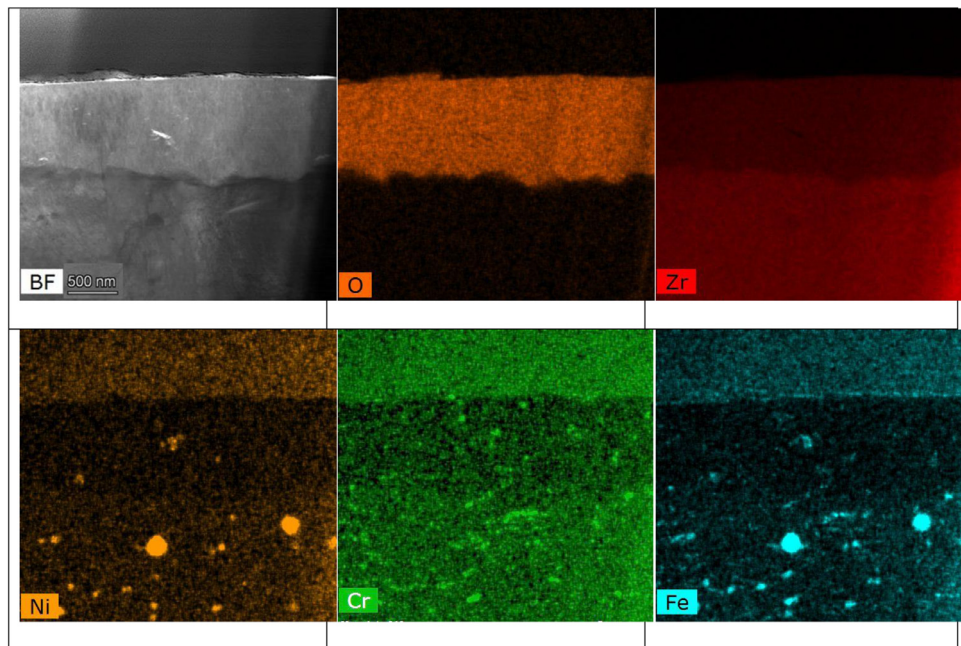


Fig. 14. TEM oxide cross section for Zirc-2 surface oxides formed after 12 months exposure in autoclave S6 or BWR NWC. The marker is 500 nm as seen in the bright field image.

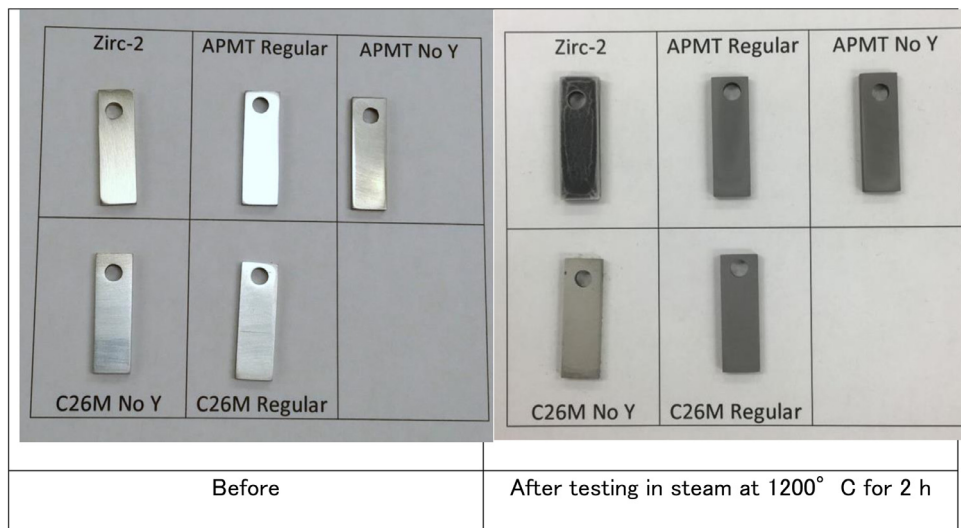


Fig. 15. Flat coupons of Zirc-2, APMT and C26M before and after testing in steam for 2 h.

2.3. Comparative water oxidation between FeCrAl and Zirc-2 cladding tubes

When Zirc-2 oxidizes in high temperature water it forms ZrO_2 which is adherent and remains mostly attached to the cladding, increasing slightly the mass of the Zirc-2 tubing as testing time increased (Figs. 2–5). However, the useful thickness of Zirc-2 metal that forms the pressure barrier between the fuel and the coolant slightly decreases. It is shown in Fig. 14 that the thickness of the oxide in the OD is approximately 1 μm , that is, the pressure bearing wall of the cladding decreased by a proportional amount which is less than 1 μm compared to the original 675 μm Zirc-2 tube wall. Opposite to Zirc-2, the mass of the tube cladding of FeCrAl (APMT and C26M) slightly loses mass as time increases (Figs. 2–4, 6, 7). Moreover, besides the mass loss, APMT would form a “thicker”

300 nm oxide on the surface of the specimens and C26M would form a “thinner” 150 nm oxide. That is, the initial wall thickness of 584 μm for APMT and 406 μm for C26M will be reduced by less than 0.5 μm due to the oxide formed on the surface. To this thickness reduction, one must add the thickness lost due to mass loss, which is 0.2 mg/cm^2 for APMT and 1 mg/cm^2 for C26M (Figs. 6 & 7). If a density of 8 g/cm^3 is assumed for both APMT and C26M, the mass loss would represent a thickness loss due to dissolution of 0.25 μm for APMT and 1.25 μm for C26M [7]. This shows that the thickness loss due to oxide formation plus dissolution for C26M would be 1.25 + 0.15 μm which is slightly higher than that for Zirc-2 tube at 1 μm after 12 months immersion. For APMT the tube wall thickness loss due to corrosion corresponds to 0.25 μm + 0.3 μm = 0.55 μm , which is approximately half of the thickness loss for Zirc-2 cladding.

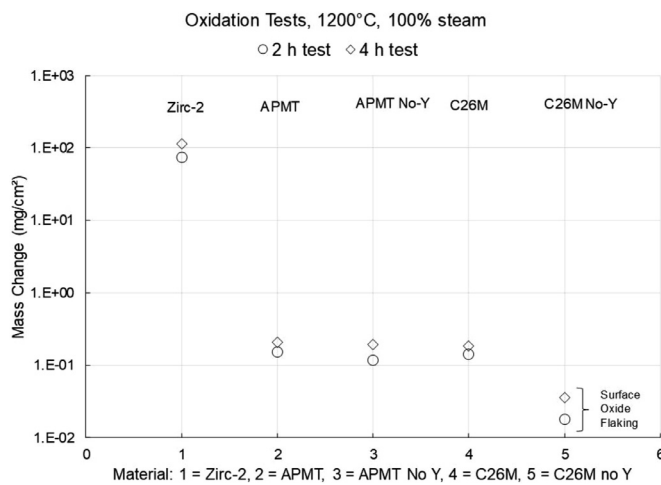


Fig. 16. Mass change for flat coupons of Zirc-2, APMT and C26M after testing in steam at 1200°C for 2 h and 4 h.

As reported before by Rebak et al [7], corrosion in high temperature does not impose limiting factor to the performance of the cladding itself since the thinning of the tube wall would be insignificant during its residence in the reactor. However, due to the large surface area of all the fuel rods in the reactor core, a small dissolution of the FeCrAl tube wall may impact the purity of water coolant [7].

2.4. Steam Resistance post Water Residence

It is well known that IronClad alloys develop a protective alumina layer on the surface when exposed to super-heated steam in the order of 1000°C or higher temperatures [5,10]. Fig. 15 shows the appearance before and after testing in steam at 1200°C of flat coupons of APMT and C26M prepared in the laboratory with

and without added yttrium to the basic composition (Table 1). Images of Zirc-2 flat coupons are also added for reference. The Zirc-2 coupon changed shape due to the heavy oxidation in steam, while both APMT coupons suffered little or no change in appearance due to the steam exposure. The C26M coupon without Y exhibited powder flaking during handling after the steam exposure. Fig. 16 shows the mass changes for coupons after 2 h and 4 h of exposure in superheated steam at 1200°C. There was little difference in the mass changes for all the coupons between 2 h and 4 h of testing. The major difference was that the Zirc-2 coupons had a mass gain of approximately 100 mg/cm² while the FeCrAl coupons had a mass gain of approximately 0.1 mg/cm² (three orders of magnitude lower for the FeCrAl). APMT had the same oxidation resistance with and without Y while C26M without Y had oxide flaking probably due to the lack of oxide adherence to the substrate. Even though C26M had oxide flaking, it still resisted the attack by steam at 1200°C.

It was important to determine if after the FeCrAl (IronClad) specimens remained in simulated reactor environment conditions for 12 months, they would still develop a protective alumina layer on the surface when exposed to accident conditions superheated steam. To elucidate this issue, tube specimens of Zirc-2, APMT, and C26M were tested in steam at 1200°C for 2 h after being in autoclave residence for 12 months. Fig. 17 shows the mass change of Zirc-2 tube specimens in the as-received (AR) (non-tested) conditions and after exposure for one year in the three autoclaves listed in Table 2. Zirc-2 specimens have similar oxidation resistance in steam both in the AR conditions and after immersion in water for up to a year. Figs. 18 and 19 show the results from steam testing of APMT and C26M, respectively. APMT had the same resistance in steam in the AR condition and after 12 months exposure to simulated reactor conditions environments (Fig. 6). Similarly, C26M offered an extraordinary resistance to attack by steam, having little or no mass change after 2 h of exposure to steam at 1200°C (Fig. 19). In the same conditions where APMT and C26M resisted attack by steam, the Zirc-2 tube coupons were fully oxidized (Figs. 17 & 20).

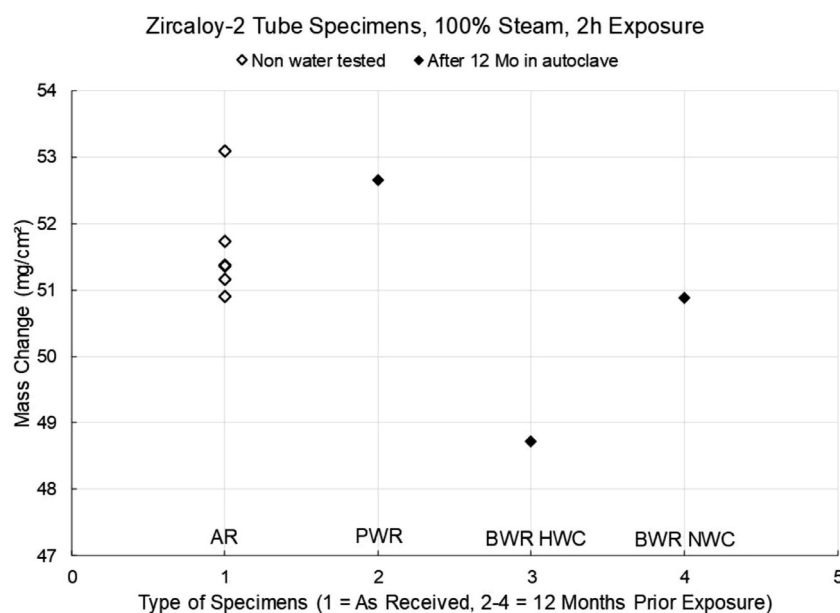


Fig. 17. Zirc-2 tube specimens tested for 2 h in steam at 1200°C show similar behavior in the AR condition and after 12 Mo immersion in three simulated reactor environments.

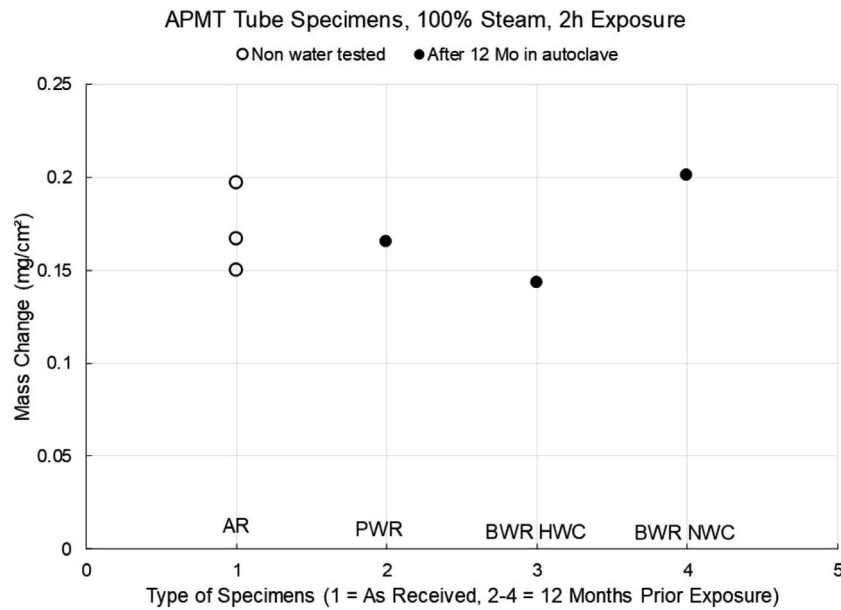


Fig. 18. APMT tube specimens tested for 2 h in steam at 1200°C show similar behavior in the AR condition and after 12 Mo immersion in three simulated reactor environments.

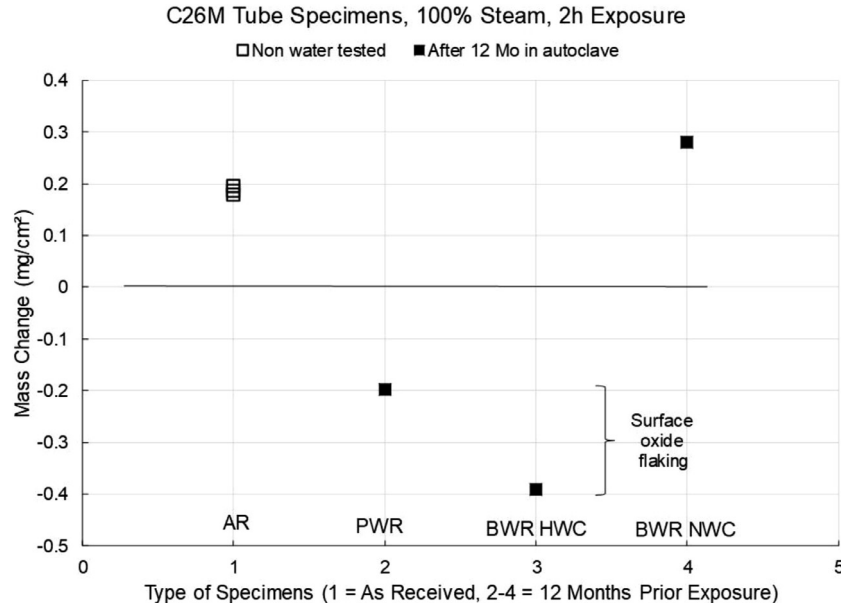


Fig. 19. C26M tube specimens tested for 2 h in steam at 1200°C show similar behavior in the AR condition and after 12 Mo immersion in three simulated reactor environments.

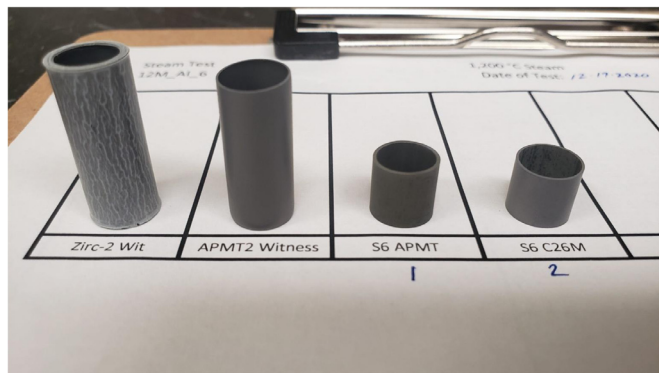


Fig. 20. Tube specimens tested for 2 h in steam at 1200°C. The two left taller specimens were as received or witness Zirc-2 and APMT. The two shorter specimens on the right had a prior exposure to the S6 autoclave (Table 2) for 12 months. Both APMT and C26M showed extraordinary resistance to attack by steam.

3. Summary and conclusions

- 1) IronClad FeCrAl alloys APMT and C26M were immersion tested for up to 12 months in three simulated reactor environment conditions. These conditions included PWR, BWR HWC and BWR NWC. Specimens of Zircaloy-2 material having the same geometrical configurations were also tested in parallel for comparison to the FeCrAl specimens.
- 2) All FeCrAl coupons has a small reduction in mass during immersion in the three environments. The amount of mass reduction was always the lowest in APMT because of its higher chromium content. Zirc-2 specimens always experienced a mass gain due to the formation of an insoluble adherent surface oxide.
- 3) During exposure in the BWR NWC, FeCrAl specimens developed double layer oxides on the surface, an external layer containing

- both Cr and Fe and a much thinner inner layer rich in Cr and Al. The inner layer is the barrier for corrosion in the ~300°C water.
- 4) After an initial small mass loss, the APMT tube specimens slowed down the recession rate while the C26M coupons continued to dissolve as the testing time increased, suggesting that the chromium oxide film on C26M was less protective than on APMT.
 - 5) After 12-month exposure to reactor simulated environments, the FeCrAl tube specimens still maintained their outstanding resistance to attack by steam at 1200°C.

Author statement

- Liang Yin: Analyzed data, XPS data, manuscript editing.
T. B. Jurewicz: 12-month immersion tests in three autoclaves S2, S5 and S6. Mass changes of water immersion tests.
M. Larsen: TEM FIBing data and analysis
M. Drobniak: SEM data and analysis
C. C. Graff: High temperature steam tests and documentation
D. R. Lutz: Data analysis and commercial side approval
R. B. Rebak: Testing matrix design, manuscript writing and editing.

Declaration of Competing Interest

The authors declare that they have no known competing financial interests or personal relationships that could have appeared to influence the work reported in this paper.

Acknowledgements

The financial support of Global Nuclear Fuels, GE Hitachi Nuclear and GE Research is gratefully acknowledged. This material is based upon work supported by the Department of Energy [National Nuclear Security Administration] under Award Number DE-NE00008823. This report was prepared as an account of work sponsored by an agency of the United States Government. Neither the United States Government nor any agency thereof, nor any of their employees makes any warranty, express or implied, or assumes any legal liability or responsibility for the accuracy, completeness, or usefulness of any information, apparatus, product, or process disclosed, or represents that its use would not infringe privately owned rights. Reference herein to any specific commercial product, process or service by trade name, trademark, manufacturer, or otherwise does not necessarily constitute or imply its endorsement,

recommendation, or favoring by the United States Government or any agency thereof. The views and opinions of authors expressed herein do not necessarily state or reflect those of the United States Government or any agency thereof.

References

- [1] C. Lemaignan, [2006], "Corrosion of Zirconium Alloy Components in Light Water Reactors," in: ASM Metals Handbook, Vol. 13C Corrosion: Environments and Industries, ASM International, Metals Park, OH, 2006, p. 415.
- [2] F Ning, X. Wang, Y. Yang, J. Tan, Z. Shang, D. Jia, X. Wu, E.-H. Han, Uniform corrosion behavior of FeCrAl alloys in borated lithium high temperature water, *J. Mater. Sci. Technol.* 70 (2021) 136–144.
- [3] S.S Raiman, K.G. Field, R.B. Rebak, Y. Yamamoto, K.A. Terrani, Hydrothermal corrosion of 2nd generation FeCrAl alloys for accident tolerant fuel cladding, *J. Nucl. Mater.* 536 (2020) (2020) 152221, doi:10.1016/j.jnucmat.2020.152221.
- [4] R.B. Rebak, Alloy Selection for Accident Tolerant Fuel Cladding in Commercial Light Water Reactors, *Metal. Mater. Trans. E* 2 (4) (2015) 197–207 December 2015 DOI 10.1007/s40553-015-0057-6.
- [5] R.B. Rebak, Iron-chrome-aluminum alloy cladding for increasing safety in nuclear power plants, *EPJ Nuclear Sci. Technol.* 3 (2017) (2017) 34 doi.org/10.1051/epjn/2017029.
- [6] R.B. Rebak, M. Larsen, Y.-J. Kim, Characterization of oxides formed on iron-chromium-aluminum alloy in simulated light water reactor environments, *Corros. Rev.* (2017) 2017, doi:10.1515/correv-2017-0011.
- [7] R.B. Rebak, T.B. Jurewicz, M. Larsen, K. Sakamoto, Immersion testing of FeCrAl tubes under simulated light water nuclear reactor normal operation conditions, in: Paper 184-30215, Top Fuel 2019 Conference, American Nuclear Society, Seattle, WA, 2019, p. 2019. September 22–27, 2019.
- [8] Rebak R. B. 2019b, Jurewicz, T. B., and Kim, Y.-J., "Electrochemical Behavior of Accident Tolerant Fuel Cladding Materials under Simulated Light Water Reactor Conditions," Advances in Electrochemical Techniques for Corrosion Monitoring and Laboratory Corrosion Measurements, ASTM STP1609, S. Papavinasam, R. B. Rebak, L. Yang, and N. S. Berke, Eds., ASTM International, West Conshohocken, PA, 2019, pp. 231–243, http://dx.doi.org/ 10.1520/STP160920170145.
- [9] R.B. Rebak, R.J. Blair, D.R. Lutz, Localized Corrosion Behavior of FeCrAl Nuclear Fuel Cladding in Pool Storage, Paper 1191-29966, Top Fuel 2019 Conference, American Nuclear Society, 2019 September 22–27, 20192019.
- [10] R.B. Rebak, in: "Accident Tolerant Materials for Light Water Reactor Fuels, Chapters 2 & 4, Elsevier, 2020, p. 2020.
- [11] K.A. Terrani, B.A. Pint, Y.-J. Kim, K.A. Unocic, Y. Yang, C.M. Silva, H.M. Meyer III, R.B. Rebak, Uniform corrosion of FeCrAl alloys in LWR coolant environments, *J. Nucl. Mater.* 479 (2016) (2016) 36–47.
- [12] K.A. Terrani, Accident Tolerant Fuel Cladding Development: Promise, Status, and Challenges, *J. Nucl. Mater.* 501 (2018) (2018) 13–30.
- [13] P. Wang, S. Grdanovska, D.M. Bartels, G.S. Was, Corrosion behavior of ferritic FeCrAl alloys in simulated BWR normal water chemistry, *J. Nucl. Mater.* 545 (2021) (2021) 152744 /10.1016/j.jnucmat.2020.152744.
- [14] W Wu, G. Ran, Y. Li, S. Cong, C. Ye, R. Zhang, Y. Sun, Early corrosion behavior of irradiated FeCrAl alloy in simulated pressurized water reactor environment, *Corros. Sci.* 174 (2020) (2020) 108824.
- [15] Y Yamamoto, B.A. Pint, K.A. Terrani, K.G. Field, Y. Yang, L.L. Snead, Development and property evaluation of nuclear grade wrought FeCrAl fuel cladding for light water reactors, *J. Nuclear Mater.* 467 (2015) (2015) 703–716 doi.org/10.1016/j.jnucmat.2015.10.019.
- [16] S.J. Zinkle, K.A. Terrani, J.C. Gehin, L.J. Ott, L.L. Snead, Accident tolerant fuels for LWRs: A perspective, *J. Nucl. Mater.* 448 (2014) (2014) 374–379.